INTEGRAL QUADRATIC CONSTRAINT-BASED ROBUSTNESS ANALYSIS OF LAUNCH VEHICLES

Felix Biertümpfel[1], Dimitrios Gkoutzos[2], David Levi[3], Jorge Valderrama[4], Harald Pfifer[5]

[1]*TU Dresden, Marschner Str. 28, 01307 Dresden, felix.biertuempfel@tu-dresden.de*
[2]*Astos Solutions GmbH, Meitnerstr. 8, 70563 Stuttgart Germany, dimitrios.gkoutzos@astos.de*
[3]*Astos Solutions GmbH, Meitnerstrasse 8, 70563 Stuttgart Germany, david.levi@astos.de*
[4]*Astos Solutions GmbH, Meitnerstrasse 8, 70563 Stuttgart Germany, jorge.valderrama@astos.de*
[5]*TU Dresden, Marschner Str. 28, 01307 Dresden, harald.pfifer@tu-dresden.de*

ABSTRACT

This paper presents the advantages of integrating linear time varying (LTV) performance analyses into the space launcher control design and certification process. Multiple performance metrics of the atmospheric flight phase for an expendable launch vehicle are analyzed for two different control strategies. The analyses cover wind disturbance and uncertainty in the launcher dynamics. A disk margin-type uncertainty is implemented to relate the analysis to classical gain and phase margins commonly used in certification processes. The uncertainties input/output behavior is covered using integral quadratic constraints. Thus, recent advances on the worst-case gain analysis of finite horizon LTV systems can be used. The corresponding analysis condition is based on a parameterized Riccati differential equation's solvability, which leads to a readily solvable nonlinear optimization problem. Using this, it is possible to explicitly respect the time varying dynamics of the space launcher in a analytical worst-case performance analysis. The applied performance certificate in combination with a sophisticated wind model provides a worst-case performance which directly compares to the nonlinear simulation. The results of a nominal and uncertain LTV analysis are compared against corresponding Monte Carlo simulations of the respective industry-sized nonlinear launcher model. These comparisons demonstrate the computational advantages and potential acceleration of the control design and certification process using LTV methods.

1 INTRODUCTION

Since the early 2000s, the NewSpace market is flourishing. A rising number of new small satellite installations led to the emergence of several micro-launcher companies. Micro launcher companies must be more responsive and flexible than the established launch services providers in order to take significant market shares. This increasing agility requires a paradigm change in the missionization process and the design of Guidance, Navigation and Control (GNC) systems. In general, both processes must accommodate for a wide range of payloads and customers. This requirement forces micro-launcher companies to abandon classical time-consuming approaches for GNC design and certification. Robust control techniques present an alternative as they promise a reduction in tuning and certification effort for new missions. Especially, in the verification and validation (V & V) process covering uncertainties and disturbances (,e.g, wind) they present a suitable complement to time consuming simulation-based methods such as Monte Carlo analysis of the full-nonlinear model. Simulation-based approaches can only provide lower bounds or probabilistic statements regarding the

worst-case performance. In contrast, analytical robustness analyses can provide actual upper bounds for the respective system.
Hence, robust control methods experience renewed interest in recent years for control design [1] and (robustness) analysis especially for the atmospheric flight phase. However, most analysis efforts consider the space launcher as linear time invariant (LTI) system using either classical phase and gain margins [2] or the structured singular value (μ-framework) [3]. However, these analyses are limited to frozen points in time and consider infinite time horizons. Hence, they fail to cover the actual launcher dynamics and finite horizon of the ascent. A nonintuitive validation gap is the consequence.
The space launcher follows a pre-calculated trajectory resulting in solely time-dependent dynamics. Linearizing the launcher dynamics along this pre-calculated trajectory thus yields a finite horizon linear time-varying (LTV) system. A recent extension of the LTV bounded real lemma (BRL) to integral quadratic constraints (IQCs) (see, e.g., [4] or [5]) presents a viable framework for the robust performance analysis of launch systems under perturbations. The LTV IQC framework presented in section 3 can cover a variety of perturbations in the launcher dynamics such as, parametric and dynamic uncertainties, hard non-linearities (, e.g., actuator saturation), and infinite dimensional systems (e.g., time delays). The general suitability of the framework for the ascent problem has been demonstrated in, e.g., [6]. Efficient computational approaches and algorithms are presented in [5] or [7].
The present paper illustrates how the LTV framework can improve and speed up a typical control design process for space launchers in atmospheric ascent. For that purpose, two classical PD controllers for the gravity turn maneuver are designed. The first controller guarantees a stable drift pole, whereas the second controller applies a drift minimal condition yielding an unstable drift pole. For both controllers, a robust performance analysis of the nominal and perturbed launcher dynamics under wind disturbance for multiple performance metrics is conducted. These metrics include the vertical drift and drift rate, pitch angle error, and aerodynamic load. The nominal LTV analysis provides fast feedback on how control design changes affect the performance metrics. The LTV IQC analysis provides fast feedback on how robust the control system is with respect to uncertainty in the launcher dynamics. Here, a disk margin-like perturbation is considered which resembles a simultaneous phase and gain perturbation. Thus, the perturbation relates back to classical robustness criteria such as gain and phase margins familiar and easy to interpret for control engineers.
An exemplary wind filter design procedure for the LTV BRL framework is presented in section 4. The proposed wind filter shapes wind disturbances matching the spectral content of Dryden-like turbulence from arbitrary norm bounded inputs . Dryden turbulence is often applied in aerospace certification. In combination with the performance certificate presented in section 3, the LTV analyses provide actual physical values which can be directly compared to the outcomes of a Monte Carlo simulation. The results of the LTV analyses are compared to equivalent Monte Carlo simulations of the nonlinear model to demonstrate the potential of the approach.
The LTV analyses presented in this paper will be an integral part of Astos Solutions' and TU Dresden's "Reconfigurable Control Design Framework for Micro-Launchers" (LAURCF) activity. Thus the paper demonstrates how customers of Astos Solutions, a provider of software and services of already more than 43 micro-launcher companies and space agencies worldwide, can in the future benefit from cutting edge research results by TU Dresden to accelerate their GNC processes.

2 GNC TOOL CHAIN AND FRAMEWORK

Following this strategy and in response to the needs of (micro-) launcher companies, Astos Solutions and TUD develop a complete toolchain making use of state-of-the-art techniques in robust control within the "Reconfigurable Control Design Framework for Micro-Launchers" (LAURCF) activity. The project LAURCF is carried out under a program of and funded by the European Space Agency

- through the “Future Launchers Preparatory Programme”. This development will bridge the gap between state-of-the-art research and industry applications for launch vehicles utilizing Astos’ unique position in the market.
The framework will encapsulate the well-established multi-purpose ASTOS software for trajectory optimization and the dynamics, kinematics and environment for the functional engineering simulator (FES). A linearization tool automatically generates linearized launch vehicle dynamics along the optimized reference trajectory and provides the possibility to extend the model by physical effects such as flexibility, sloshing, Tail-Wags-Dog (TWD), jet damping and more. This provides a significant benefit allowing the GNC engineer to adjust the complexity of the model to the corresponding task. A linearization verification tool validates the obtained linearized dynamics against the nonlinear FES and provides immensely beneficial rapid insights to the GNC engineer. One of the key parts of the control design cycle is to introduce and satisfy control requirements. In robust control, these requirements are typically included as weighting functions. The requirements specification tool based on the approach developed by TUD [8] offers a straightforward interpretation and translation of these requirements into the design of the weighting functions. This approach overcomes the need for expert knowledge and experience acquired over years and aims to make robust control more accessible to the industry. The robust control synthesis tool allows to efficiently implement different types of controllers, such as structured and non-structured H_∞, LTV and LPV controller including observer-based architectures with predefined structures [9], [10]. Apart from classical stability analyses and robust analyses for LTI systems, the robust control analysis tool offers nominal and integral quadratic constraint (IQC) based worst-case analyses for LTV systems [7], as described - in a reduced form - in this paper. A Monte Carlo (MC) environment linking the uncertainties defined in the models for the robust control design to the FES completes the framework, providing the user the final step in the verification and validation (V & V) process by straightforward performing and post-process MC simulations.

3 UNCERTAIN LINEAR TIME-VARYING SYSTEMS OVER FINITE HORIZONS

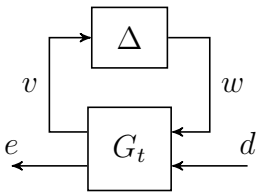

Figure 1: Interconnection of an LTV system and perturbation

An uncertain linear time-varying system $F_u(G_t, \Delta)$ is defined by the feedback interconnection of a nominal LTV system G_t and the perturbation Δ as pictured in Fig. 1. The nominal LTV system G_t is given by:

$$\begin{aligned} \dot{x}_{G_t}(t) &= A_{G_t}(t)x_{G_t}(t) + B_{G_t}(t)\begin{bmatrix} w(t) \\ d(t) \end{bmatrix} \\ \begin{bmatrix} v(t) \\ e(t) \end{bmatrix} &= C_{G_t}(t)x_{G_t}(t) + B_{G_t}(t)\begin{bmatrix} w(t) \\ d(t) \end{bmatrix}. \end{aligned} \tag{1}$$

In (1), $x_{G_t}(t) \in \mathbb{R}^{n_{x_{G_t}}}$, $d(t) \in \mathbb{R}^{n_d}$, and $e(t) \in \mathbb{R}^{n_e}$ denote the state, input, and the output vector, respectively. The matrices A_{G_t}, B_{G_t}, C_{G_t}, and D_{G_t} are piecewise continuous locally bounded matrix-valued functions of time with corresponding dimensions. To shorten the notation, the explicit time dependence is mostly omitted in this paper. Thus, LTI systems will be clearly introduced as such. The uncertainty $\Delta : L_2^{n_v}[0,T] \to L_2^{n_w}[0,T]$ is a bounded and causal operator. Δ can describe hard nonlinearities like saturations, infinite-dimensional operators like time delays, and dynamic and real parametric uncertainties.

3.1 Integral Quadratic Constraints

In this paper, the input output behavior of a perturbation Δ is bounded via time-domain IQCs. Time domain IQCs are defined based on a filter $\Psi \in \mathbb{RH}_\infty^{n_z \times (n_v + n_w)}$ and a $n_z \times n_z$ real, symmetric matrix M [11]. In case the output z of the filter Ψ fulfills the quadratic time constraint

$$\int_0^T z(t)^T M z(t)\, dt \geq 0 \tag{2}$$

for all $v \in L_2[0,T]$ and $w = \Delta(v)$ over the interval $[0,T]$, the uncertainty Δ satisfies the IQC defined by M and Ψ. If so, the short notation $\Delta \in IQC(\Psi, M)$ is used.

3.2 Robustness Analysis of Linear Time-Varying Systems

From the worst-case analysis of nominal LTV systems in [12] and the finite horizon time-domain IQC formulation of the perturbation Δ, a worst-case gain condition can be derived [5], [13]. It provides a guaranteed upper bound on the input-output behavior of an uncertain LTV systems over the considered finite analysis horizon. Thus, it is possible to tackle the analysis problem posed by the interconnection of a known LTV system G_t and a perturbation Δ. Given a perturbation satisfying an IQC represented by (Ψ, M), i.e. $\Delta \in IQC(\Psi, M)$, the interconnection $F_u(G_t, \Delta)$ can be extended by the IQC filter Ψ. This procedure is illustrated by Fig. 2. The dynamics of this interconnection are represented by

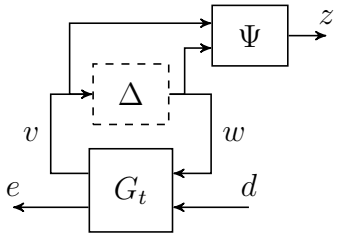

Figure 2: Feedback Interconnection LTV system G_t and uncertainty Δ

$$\begin{aligned} \dot{x}(t) &= A(t)\, x(t) + \begin{bmatrix} B_1(t) & B_2(t) \end{bmatrix} \begin{bmatrix} w(t) \\ d(t) \end{bmatrix} \\ \begin{bmatrix} z(t) \\ e(t) \end{bmatrix} &= \begin{bmatrix} C_1(t) \\ C_2(t) \end{bmatrix} x(t) + \begin{bmatrix} D_{11}(t) & D_{12}(t) \\ D_{21}(t) & D_{22}(t) \end{bmatrix} \begin{bmatrix} w(t) \\ d(t) \end{bmatrix}. \end{aligned} \tag{3}$$

denoted as the extended LTV system G. In (3), $x(t) \in \mathbb{R}^{n_x}$ represents the state vector containing the states of G_t and Ψ, $d(t) \in \mathbb{R}^{n_d}$ the disturbance vector, and $e(t) \in \mathbb{R}^{n_e}$ the performance output vector. By enforcing the time-domain inequality (2) on the filter output z, the explicit representation of the uncertainty $w = \Delta(v)$ is replaced. The finite horizon worst-case $L_2[0,T]$ to Euclidean gain is proposed as:

$$\|F_u(G_t, \Delta)\|_2 := \sup_{\Delta \in \text{IQC}(\Psi, M)} \sup_{\substack{d \in L_2[0,T] \\ d \neq 0, x(0)=0}} \frac{\|e(T)\|_2}{\|d(t)\|_{2[0,T]}}. \tag{4}$$

This gain can be geometrically interpreted as the ball upper bounding the worst-case output $e(T)$ at the terminal time T over all $\Delta \in IQC(\Psi, M)$ given $\|d(t)\|_{2[0,T]} = 1$, with

$$\|d\|_{2[0,T]} = \left[\int_0^T d^T(t) d(t)\, dt \right]^{\frac{1}{2}}. \tag{5}$$

A dissipation inequality can be stated to upper bound the worst-case $L_2[0,T]$ to Euclidean gain of the interconnection $F_u(G_t,\Delta)$. It is based on the extended LTV system G given by (3) and the finite horizon time domain IQC formulation in (2). For a more thoroughly description the reader is referred to [5] and [13]. This dissipation inequality is rearranged as an equivalent Riccati differential equation (RDE) formulation in the following Theorem:

Theorem 1. *Let $F_u(G_t,\Delta)$ be well posed $\forall\,\Delta \in IQC(\Psi,M)$, then $\|F_u(G_t,\Delta)\|_2 < \gamma$ if there exists a continuously differentiable symmetric $P:[0,T]\to\mathbb{R}^{n_x\times n_x}$ such that*

$$P(T) = \frac{1}{\gamma}C_2(T)^T C_2(T), \tag{6}$$

$$\dot{P} = Q + P\tilde{A} + \tilde{A}^T P - PSP \qquad \forall t\in[0,T], \tag{7}$$

and

$$R = \begin{bmatrix} D_{11}^T M D_{11} & D_{11}^T M D_{12} \\ D_{12}^T M D_{11} & D_{12}^T M D_{12} - \gamma I \end{bmatrix} < 0 \,\forall\, t\in[0,T], \tag{8}$$

with

$$\tilde{A} = \begin{bmatrix} B_1 & B_2 \end{bmatrix} R^{-1} \begin{bmatrix} (C_1^T M D_{11})^T \\ (C_1^T M D_{12})^T \end{bmatrix} - A, \quad S = -\begin{bmatrix} B_1 & B_2 \end{bmatrix} R^{-1} \begin{bmatrix} B_1^T \\ B_2^T \end{bmatrix} \tag{9}$$

and

$$Q = -C_1^T M C_1 + \begin{bmatrix} (C_1^T M D_{11})^T \\ (C_1^T M D_{12})^T \end{bmatrix}^T R^{-1} \begin{bmatrix} (C_1^T M D_{11})^T \\ (C_1^T M D_{12})^T \end{bmatrix}. \tag{10}$$

Proof. The proof is provided in [5]. □

The RDE (7) is a stiff ordinary differential equation [14]. Thus, in this paper it is solved with the Matlab internal solver `ODE15s` [15]. The computational effort scales with the length of the analysis horizon as well as the complexity/size of the IQC parameterization. Especially the latter makes the RDE numerically harder to solve, due to adverse effects on its conditioning.

3.3 Worst-Case Gain Computation

Generally, an infinite number of IQCs exist to describe a given uncertainty. The most common approach found in literature, see, e.g., [16] or [17], is to select a fixed filter Ψ and parameterize M. This means the IQC matrix M is confined to a feasibility set $\mathcal{M}$ such that $\Delta\in IQC(\Psi,M)$ for all $M\in\mathcal{M}$. The analysis conducted in this paper covers perturbations in the form of full-block LTI dynamic uncertainties. An example for a feasible parameterization of such an uncertainty type is shown in Example 3.1.

Example 3.1. *Let Δ be a full-block LTI dynamic uncertainty, with $\Delta\in\mathbb{RH}_\infty$ and $\|\Delta\|_\infty \le b\in\mathbb{R}$. A valid time-domain IQC for Δ is defined by $\Psi = \left[\begin{smallmatrix} b\psi_\nu\otimes I_{n_v} & 0 \\ 0 & \psi_\nu\otimes I_{n_v}\end{smallmatrix}\right]$ and $\mathcal{M} := \{M = \left[\begin{smallmatrix} X\otimes I_{n_v} & 0 \\ 0 & -X\otimes I_{n_v}\end{smallmatrix}\right] : X = X^T > 0 \in \mathbb{R}^{(\nu+1)\times(\nu+1)}\}$. A typical choice for $\psi_\nu\in\mathbb{RH}_\infty^{(\nu+1)\times 1}$ is:*

$$\psi_\nu = \begin{bmatrix} 1 & \frac{s+\rho}{s-\rho} & \dots & \frac{(s+\rho)^\nu}{(s-\rho)^\nu} \end{bmatrix}^T,\ \rho<0\,,\ \nu\in\mathbb{N}_0. \tag{11}$$

In the example above, the matrix variables X and Y are free parameters, whereas ψ_ν is a fixed basis function with preselected ν and ρ. By $\otimes$, the Kronecker product is denoted.
By following the described approach, the RDE in Theorem 1 is now parameterized with $M \in \mathcal{M}$. This leads to the corresponding nonlinear optimization problem to minimize γ [4]:

$$\begin{aligned} &\min_{M \in \mathcal{M}} \gamma \\ &\text{such that } \forall t \in [0, T] \\ &\qquad P(T) = \frac{1}{\gamma} C_2(T)^T C_2(T) \\ &\qquad \dot{P} = Q + P\tilde{A} + \tilde{A}^T P - PSP \\ &\qquad R < 0. \end{aligned} \tag{12}$$

In [7], an algorithm to efficiently solve the optimization problem is given. This algorithm is based on two nested loops identifying M such that γ is a minimum. In the inner loop, a bisection for a fixed M over γ is conducted. The corresponding outer loop performs a global optimization over $M \in \mathcal{M}$ applying the Log-L-SHADE [7] meta-heuristic identifying the minimal γ. The algorithm provides a set of parameters which allow to adjust it to a specific analysis. These include the search space of the decision variables, the initial population size, i.e. the number of randomized initial guesses in the search space, and amount of population iterations, i.e. the number of decision set iterations. The latter two, in general, scale with the number of decision variables. For more details on recommended settings and their effects the reader is referred to [7].

4 LAUNCHER MODEL

In this paper, multiple performance metrics of an expendable launch vehicle (ELV) in atmospheric ascent under wind disturbance are analyzed. The respective time horizon relevant for the analysis spans from $t_s = 25\,\text{s}$ to $t_f = 95\,\text{s}$ after lift-off.

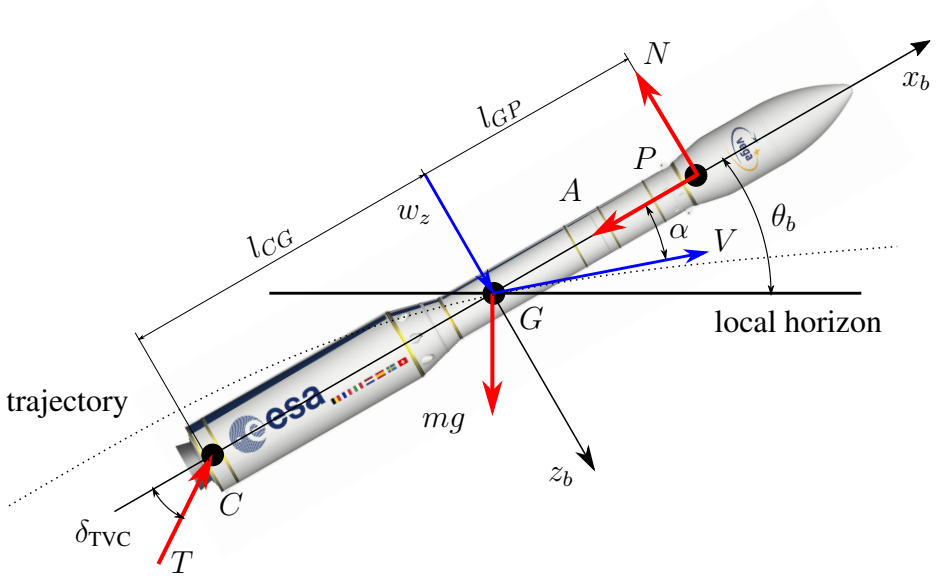

Figure 3: Expandable launch vehicle in body fixed reference frame

4.1 Nonlinear Dynamics

During the atmospheric ascent, the space launcher can be treated as perfectly symmetric, with fully decoupled pitch and yaw dynamics for small roll-rates [18]. In the present paper, only the pitch dynamics are further considered. Given the flight segment's overall duration and velocity regime, the earth can be assumed flat and non-rotating [19]. The analysis only considers the rigid body motion. Fuel sloshing is neglected as only the upper module uses liquid propellant. Hence, liquid fuel makes up only a negligible fraction of the overall system mass. By the same reasoning, the effects of nozzle inertia are neglected. An illustration of the launcher's pitch dynamics is given in Fig. 3. Forces are indicated by red and velocities by blue arrows.
The launcher's nonlinear equations of motion (EoM) are formulated with respect to its instantaneous center of gravity G in a body-reference coordinate system denoted by the subscript b. The x_b-axis is aligned with the launcher's symmetry axis and is defined positive in the direction of forward travel. The z_b-axis points downward, forming a right-hand system with the y_b-axis. The launcher's nonlinear EoM in the pitch plane are described by:

$$\begin{aligned}
\ddot{\theta}_b(t) =& \frac{\sum M_y(Ma,\alpha,h,t)}{J_{yy}(t,m)} \\
=& \frac{N(Ma,\alpha,h,t) l_{GP}(Ma,m,t)}{J_{yy}(t,m)} - \dot{\theta}_b \frac{\dot{J}_{yy}(m,t)}{J_{yy}(m,t)} - \frac{T(t) l_{CG}(t,m)}{J_{yy}(t,m)} \sin\delta_{\text{TVC}}(t) \\
\ddot{x}_b(t) =& \frac{\sum F_x(Ma,\alpha,h,t)}{m(t)} - \dot{\theta}_b(t)\dot{z}_b(t) \\
=& \frac{T(t)\cos\delta_{\text{TVC}}(t) - A(Ma,\alpha,h,t)}{m(t)} - g_0(h)\sin\theta_b(t) - \dot{\theta}_b(t)\dot{z}_b(t) \\
\ddot{z}_b(t) =& \frac{\sum F_z(Ma,\alpha,h,t)}{m(t)} - \dot{\theta}_b(t)\dot{x}_b(t) \\
=& -\frac{N(Ma,\alpha,h,t)}{m(t)} - \frac{T(t)}{m(t)} \sin\delta_{\text{TVC}}(t) + g_0(h)\cos\theta_b(t) - \dot{\theta}_b(t)\dot{x}_b(t)
\end{aligned} \tag{13}$$

In (13), $\sum M_y$ is the sum of moments around the pitch axis formulated with respect to the center of gravity G. The sum of forces in x_b and z_b direction are denoted by $\sum F_x$ and $\sum F_z$, respectively. The launcher's pitch angle corresponds to the angle between the x_b axis and the local horizon. It is denoted θ_b. The axial and normal accelerations are denoted $\ddot{x}_b$ and $\ddot{z}_b$. Finally, A and N are the axial and normal aerodynamic forces. They are defined by

$$\begin{aligned}
A(Ma,\alpha,h,t) &= Q(h,t)\, S_{\text{ref}}\, C_A(\alpha, Ma) \\
N(Ma,\alpha,h,t) &= Q(h,t) S_{\text{ref}}\, C_N(\alpha, Ma),
\end{aligned} \tag{14}$$

with the dynamic pressure $Q(h,t) = 0.5\rho(h)V^2(t)$, reference area S_{ref} and aerodynamic force coefficients C_A and C_N. These coefficients dependent nonlinearly on the Mach number Ma and the angle of attack α and act on the launcher's center of pressure P. The variable V is the absolute aerodynamic velocity of the ELV. The density of the air ρ is calculated according to the international standard atmosphere (ISA) [20]. In contrast to standard aerospace conventions, the aerodynamic forces are expressed in body axes rather than in a coordinate system attached to the aerodynamic velocity. Here, the axial and normal forces are defined in the negative axis directions. Thus, A acts in negative x_b direction and N acts in negative z_b direction In (14), the angle of attack is approximated as

$$\alpha(t) \approx \frac{\dot{z}_b(t) - w_z(t)}{\dot{x}_b(t)}, \tag{15}$$

where w_z is the external wind disturbance aligned with the z_b-axis.
The launcher's thrust T acts at the nozzle reference point C. It can be rotated by the angle δ_{TVC} using the thrust vector control (TVC) system. The TVC deflection presents the launcher's sole means of control. Due to the characteristics of the solid rocket motor, the thrust follows a predefined time profile after ignition.
The overall moment of inertia J_{yy} is defined with respect to the instantaneous center of gravity G and depends directly on the launcher's momentary mass. The same is true for the center of gravity itself. The altitude-dependent gravitational acceleration $g_0(h)$ is calculated based on the world geodetic system 84 (WGS 84) [21] with a launch site close to the equator.
A second-order transfer function with unit DC-gain k_{TVC}, natural frequency $\omega_{\text{TVC}} = 50\,\text{rad/s}$, and damping ratio $\zeta_{\text{TVC}} = 0.7$ is used to model the dynamics of the thrust vector control system:

$$\begin{bmatrix} \dot{\delta}_{\text{TVC}} \\ \ddot{\delta}_{\text{TVC}} \end{bmatrix} = \begin{bmatrix} 0 & 1 \\ -\omega_{\text{TVC}}^2 & -2\zeta_{\text{TVC}}\omega_{\text{TVC}} \end{bmatrix} \begin{bmatrix} \delta_{\text{TVC}} \\ \dot{\delta}_{\text{TVC}} \end{bmatrix} + \begin{bmatrix} 0 \\ k_{\text{TVC}}\omega_{\text{TVC}}^2 \end{bmatrix} \delta_{\text{TVC,c}} \tag{16}$$

The TVC dynamics are connected to the launch vehicle rigid body dynamics via δ_{TVC}. The commanded TVC deflection $\delta_{\text{TVC,c}}$ remains the sole control input.

4.2 Linear Dynamics

The nominal trajectory of a space launcher through the earth's atmosphere is usually a so-called gravity turn. It is calculated under the paradigm that only a velocity component in x_b-direction shall exist, i.e., $\alpha = 0$. Hence, the normal acceleration due to curvature of the launcher trajectory and the gravitational acceleration on the launcher must compensate each other. The balance of both forces leads to the set of equations [22]:

$$\begin{aligned} \dot{h} &= V \sin\theta_b & \dot{X} &= V \cos\theta_b \\ \dot{V} &= \frac{T - D}{m} - g_0 \sin\theta_b & \dot{\theta}_b &= -\frac{g_0}{V} \cos\theta_b \end{aligned} \tag{17}$$

derived from the launcher's equations of motion (13). In (17), h is the altitude and D is the downrange distance. Solving (17) for a given h_0, θ_0, $\dot{x}_{b_0}$ and D_0 provides a so-called pitch program for the launcher.
The performance analysis in section 3 requires an LTV representation of the ELV along the reference gravity turn trajectory. In this paper, the finite horizon LTV model is calculated by numerically linearizing the nonlinear dynamics in (13) with respect to a trajectory fixed frame, see, for example, [23] for details. The time segment spans from $25\,\text{s}$ to $95\,\text{s}$ after lift-off and a step size of $0.1\,\text{s}$ is chosen. The result is a finite horizon LTV system G_t as defined in (1). The state vector including the linear actuator dynamics is $x = [\Delta\theta, \Delta\dot{\theta}, \Delta\dot{z}, \Delta\delta_{\text{TVC}}, \Delta\dot{\delta}_{\text{TVC}}]^T$, the disturbance vector is $d = \Delta w_z$, the input vector is $u = \Delta\delta_{\text{TVC,c}}$, and the output vector is $y = [\Delta\theta, \Delta\dot{\theta}, \Delta\dot{z}, \Delta z, \Delta Q\alpha, \Delta\alpha]^T$. Note that the $\Delta\dot{x}$ state is truncated due to its neglectable influence following common practice [23]. The symbol Δ refers to the deviation from the reference value on the design trajectory.

4.3 Wind Model

The evaluated wind disturbance shall resemble Dryden turbulence profiles. These are frequently used aerospace certification processes, see, for example, [24].

4.3.1 Wind Filter Nonlinear Analysis

In the nonlinear analysis, the Dryden wind filter G_w for vertical turbulence

$$\begin{aligned} \dot{x}_w(t) &= \begin{bmatrix} 0 & 1 \\ -\left(\frac{V(t)}{L_w}\right)^2 & -2\frac{V(t)}{L_w} \end{bmatrix} x_w(t) + \begin{bmatrix} 0 \\ \left(\frac{V(t)}{L_w}\right)^2 \end{bmatrix} n_w(t) \\ w_z(t) &= \begin{bmatrix} \sigma(h)\sqrt{\frac{L_w}{\pi V(t)}} & \sigma(h)\frac{L_w}{V(t)}\sqrt{\frac{3L_u}{\pi V(t)}} \end{bmatrix} x_w(t) \end{aligned} \tag{18}$$

with white noise input n_w, is used to generate the wind disturbance w_z. Here, the white noise signal is calculated by Matlab's internal band-limited white noise block. These signals have a power spectral density Φ of one and are shaped into continuous turbulence profiles statistically matching real turbulence by the filter G_w. In (18), V is the launcher's velocity, σ is the altitude-dependent turbulence intensity, and L_w is the turbulence scale length. For the analysis, the values for σ are interpolated over altitude, based on the data for severe turbulence provided in [25]. Contrary to [25], the turbulence scale length is chosen to five-times the recommended value, i.e. $L_w = 2629.2\text{m}$. This results in longer turbulence gusts, which are more critical in the context of the analyzed trajectory disturbances. According to the analyzed trajectory segment, the value of L_u is not altitude dependent following [25].

4.3.2 Wind Filter Linear Analysis

As a consequence of the discussed norm bound on the input disturbance signal imposed by the strict BRL, the Dryden wind filter in (18) cannot directly be implemented in the LTV analysis. In [26], a corresponding modification of the Dryden filter is introduced. It consists of a pre-filter (high-pass) and a scaled LTV formulation of the Dryden filter (18) $G_{w,\text{LTV}}$:

$$\begin{aligned} \dot{x}_w(t) &= \begin{bmatrix} 0 & 1 \\ -\left(\frac{V(t)}{L_w(t)}\right)^2 & -2\frac{V(t)}{L_w(t)} \end{bmatrix} x_w(t) + \begin{bmatrix} 0 \\ \left(\frac{V(t)}{L_w(t)}\right)^2 \end{bmatrix} d(t) \\ w_z(t) &= k_w \begin{bmatrix} \sigma(t)\sqrt{\frac{L_w(t)}{\pi V(t)}} & \sigma(t)\frac{L_w(t)}{V(t)}\sqrt{\frac{3L_w(t)}{\pi V(t)}} \end{bmatrix} x_w(t). \end{aligned} \tag{19}$$

The time constant is increased to $15\,\text{s}$ to account for the larger turbulence scale length. Using $G_{w,\text{LTV}}$ in combination with the pre-filter, the wind disturbance w_z in the LTV worst case analysis resulting from filtering the norm bounded worst case wind input signal d by $G_{w,\text{LTV}}$ has comparable frequency content and amplitudes as real turbulence.

5 EXAMPLE DESIGN PROCESS INCLUDING LINEAR TIME-VARYING ANALYSES

This section presents an exemplary design process for a space launcher pitch controller. The use of LTV methods to speed up and enhance the design process by providing fast and reliable feedback during tuning is demonstrated.

5.1 Control Design

A control system is required to stabilize the inherently unstable launcher dynamics while following the pitch program. A proportional-derivative (PD) control law is used in the θ channel. Proportional $\dot{\theta}$ feedback realizes the derivative part which avoids a derivative filter. The α channel only employs proportional feedback yielding the complete control law:

$$\delta_{\text{TVC,cmd}} = -K_{\text{TVC}}(K_{\dot{\theta}}\Delta\dot{\theta} + K_{\theta}\Delta\theta + K_{\alpha}\Delta\alpha), \tag{20}$$

where K_{TVC} is the TVC servo-amplifier, $K_{\dot{\theta}}$ the rate gyro, K_{θ} the orientation gyro, and K_{α} the angle of attack sensor gain. No gain-scheduling is employed. This particular control scheme is chosen as

Table 1: Controller gains used for the analysis

Controller	K_{TVC}	$K_{\dot{\theta}}$	K_{θ}	K_{α}
Stable	1.2	0.4	1.5	0.15
Unstable	0.8	0.4	1.0	1.6

it minimizes the vertical trajectory drift under wind disturbance. Two sets of gains are calculated following [27, Chapter 3]. The first set corresponds to stable closed loop dynamics over the whole trajectory. The second set provides closed loop dynamics with an unstable flight path pole along the complete ascent. This design relates to a so called drift minimal condition and promises significantly better drift performance. Both designs have comparable closed loop bandwidth along the trajectory (ranging from $5.2\,\text{rad/s}$ to $8.4\,\text{rad/s}$). Table 1 summarizes the two gain sets. The performance of both controllers has to be evaluated to chose a design and proceed with the development process. As one of the closed loop systems is unstable, classical LTI methods are not applicable. Hence, simulation-based methods like Monte Carlo simulations present the only viable option in industry today. Finite horizon LTV analyses are not restricted to "stable" dynamics and can therefore present a valuable complement to simulation-based methods.

5.2 Analysis Setup

The general analysis structure for the proposed control design is shown in Fig. 4. In the nonlinear

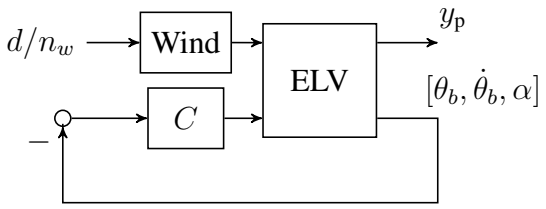

Figure 4: General analysis interconnection used for nominal launcher analysis

analysis, the ELV-block is described by the nonlinear dynamics (13) in section 4.1. Additionally, the Wind-block represents the unscaled wind filter G_w, with white noise input $n_w(t)$. Depending on the test case, block C represents the stabilizing or non-stabilizing controller with the gains provided in Tab. 1. Identical controllers are used in the linear and nonlinear analyses. Furthermore, the performance output y_{p} includes the signals $\Delta Q\alpha$ (aerodynamic load), $\Delta\theta$ (pitch angle deviation), $\Delta\dot{z}$ (vertical drift rate), and Δz (vertical deviation form trajectory).
In case of the LTV analyses, the ELV-block describes the linear dynamics in introduced in section 4.2. Furthermore, the scaled wind filter $G_{w,\text{LTV}}$ with pre-filter is applied with input d.

5.3 Nominal Performance Analysis

A nominal formulation of Theorem 1 (see, e.g., [12]) is used to calculate the nominal finite horizon worst-case $L_2[0,T]$ to Euclidean gain. The (nominal) finite horizon worst-case $L_2[0,T]$ to $\|e(T)\|_2$ gain can only upper bound the performance output y_{p} at the respective terminal time T. Therefore, it is necessary to analyze a set of terminal times covering the trajectory. The LTV analysis is performed on final times T_i in the interval $[30\,\text{s}, 95\,\text{s}]$ with a step size of 5s. For this grid, the scalings k_{w_i} of $G_{w,\text{LTV}}$ for each time interval $[0, T_i]$ are calculated by the procedure proposed in [26]. The upper bound γ on the nominal performance metric is based on the existence of the nominal form of the RDE in (7)

Table 2: Comparison of worst-cases identified by LTV and most critical Monte Carlo analysis results (MC)

	$Q\alpha$[Pa°]		$\Delta\theta$[°]		$\Delta\dot{z}$[m/s]		Δz[m]	
	LTV	MC	LTV	MC	LTV	MC	LTV	MC
$K_\alpha = 0.15$	$4.6 \cdot 10^5$	$1.8 \cdot 10^5$	1.9	0.8	18.2	9.9	409.7	327.7
$K_\alpha = 1.6$	$2.6 \cdot 10^5$	$1.0 \cdot 10^5$	5.1	1.9	3.4	1.7	153.3	72.0

over the full horizon $[0, T]$. Thus, the worst-case γ can be easily calculated via bisection.The RDE is solved using the Matlab internal `ode15s` solver for stiff ordinary differential equations (ODEs) using its default settings. Fig. 5 shows the results of the LTV analysis for both control designs. The points in time in-between the analysis grid are linearly interpolated.

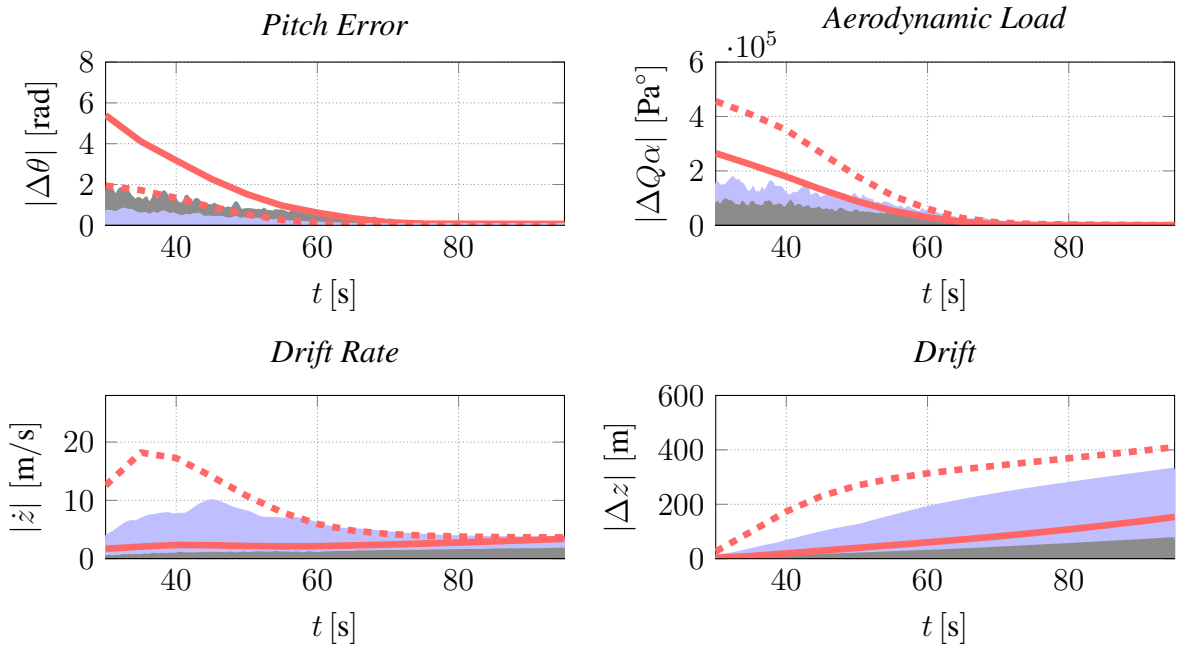

Figure 5: Nominal analysis results: Monte Carlo drift minimal (—), LTV drift minimal (—), Monte Carlo stabilizing controller (—), LTV stabilizing controller (- - -)

The LTV analysis provides direct feedback on the influence of the controller design updates. A comparison of the results for both controllers (summarized in Tab. 2) shows a noticeable reduction in the maximal drift and drift rate from the trajectory in the nonlinear analysis (Δ refers to the deviation from the values on the nominal trajectory at a time t). The calculated worst-case drift rate and drift reduce from to $18.2\,\mathrm{m/s}$ to $3.4\,\mathrm{m/s}$ and $409.7\,\mathrm{m}$ to $153.3\,\mathrm{m}$, respectively using the drift minimizing design. This relates to a reduction of the drift and trajectory offset by a factor of 5.4 and 2.7, respectively. As the launcher actively steers into the wind, the maximum pitch angle error $\Delta\theta$ increases from $1.9°$ to $5.1°$. The maximum aerodynamic load reduces using the non-stabilizing controller from $4.6 \cdot 10^5$Pa° to $2.6 \cdot 10^5$Pa°. The main reason is that the controller steers the launcher into the wind reducing the angle of attack α. The complete LTV analysis was finished in $3\,\mathrm{min}$ using a standard desktop computer.

Afterwards, a Monte Carlo simulation of the nonlinear model is conducted in Matlab Simulink using the corresponding analysis interconnection in Fig. 4. The simulation starts at $t_\mathrm{s} = 25\mathrm{s}$ and ends at $t_\mathrm{f} = 95\mathrm{s}$ after lift-off. 5000 unique white noise signals $n_{w_i}(t)$ are evaluated. This analysis took 2h10min on the same computer for this relatively small disturbance set. Fig. 5 compares the MC

results to the LTV analysis. The LTV worst-case envelopes encloses all signals of the Monte Carlo simulation. Focusing on the stabilizing controller. The Monte Carlo results for $\Delta Q\alpha$ and $\Delta\theta$ for time after $60\,\mathrm{s}$ are almost identical to the corresponding LTV worst-cases, which upper bounds the MC with by narrow margin. The reducing wind influence causes the narrowing margin. Regarding the non-stabilizing controller, the LTV provides an upper bound for all performance metrics. As can be seen from Tab. 2, the LTV analysis predicts the influence of control design changes with good accuracy. For example, the drift reduces by a factor of 4.6 using the drift minimizing design, which is close to the predicted factor of 2.7. The degradation in drift rate performance by a factor of 5.8 is also well predicted by the LTV analysis. The latter also yields a degradation of 5.4. Thus, the finite horizon LTV approach demonstrates its suitability for analyzing unstable dynamics and providing a fast estimate of the system performance as it accurately matches the actual system's behavior. Moreover, the LTV analysis predicts the relative changes in performance between the two control designs with high accuracy.
It can be concluded that the nominal LTV analysis provides direct and reliable feedback on the influence of controller design changes. This feedback is provided in a matter of minutes rather than hours. Thus, significantly more control designs can be analyzed in the same amount of time leading to a more efficient control design process.

5.4 Robust Performance Analysis

The next step after choosing the preferred drift-minimal control design is to evaluate its robustness with respect to perturbations in the system dynamics. Common robustness measurements include classical gain and phase margins. These margins quantify the maximum (individual) gain or phase perturbation that a single closed-loop may withstand before becoming unstable. They do not require specific, detailed uncertainty models and, hence, these margins are easy to evaluate. Additionally, engineers have significant experience on the interpretation of the analysis results. Symmetric disk margins (see, e.g., [28]) permit simultaneous perturbations in both gain and phase inside a predetermined disk. It is typical to simply evaluate these types margins at "frozen" points along the trajectory using LTI methods. However, this fails to capture the nature of the ascent problem and prohibit unstable dynamics and thus the drift minimal design entirely.
However, a disk margin-like perturbation can be easily integrated into the closed loop using a dynamic uncertainty Δ, with $\|\Delta\|_\infty \leq b \in \mathbb{R}^+$. The norm bound b of Δ relates to a gain perturbation of in the interval $[\frac{1-b}{1+b}, \frac{1+b}{1-b}]$. The simultaneous phase perturbation is confined to the interval $[-2\tan^{-1} b, 2\tan^{-1} b]$. Hence, this perturbation type can be analyzed inside the IQC LTV framework relating to a "classical" margin analysis with easy interpretable results. Fig. 6 displays the analysis interconnection for an input disk margin. Besides adding the disk-margin interconnection, the analysis

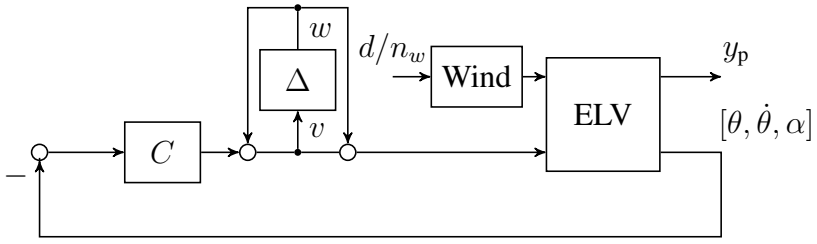

Figure 6: General analysis interconnection for margin analysis

setup remains unchanged compared to section 5.2. However, only the drift and drift rate are analyzed for brevity.

The interconnection in Fig. 6 has to be transfered into the IQC framework as described in Section 3.2. The dynamic LTI uncertainty Δ is represented by the IQC description from Example 3.1. For the present analysis, ρ is chosen to -1 and ν to 0.01.
As its nominal equivalent, the finite horizon worst-case $L_2[0, T]$ to Euclidean gain can only upper the performance signal at the final time T. Thus, the same restrictions apply and the performance is evaluated at on the same analysis grid. The analysis is repeated for increasing uncertainty norm bounds to evaluate the performance degradation of the system. The norm bounds increase from $b = 0.10$ by a step size of 0.01 until the algorithm fails to provide a feasible γ on an interval $[0, T_i]$. The latter corresponds to the performance metric growing out of bounds indicating a departure of the launcher.
The Log-L-Shade algorithm calculates the respective upper bounds $\Delta z_{\mathrm{WC},i}$ and $\Delta z_{\mathrm{WC},i}$ for a given b and T_i. Fig. 7 shows the LTV IQC analysis results, where points in-between the analysis grid are linearly interpolated. The maximum b for which the analysis can be completed is 0.16. This value corresponds to a simultaneous gain and phase perturbation of $\pm 2.8\,\mathrm{dB}$ and $\pm 18.2°$, respectively. For $b = 0.17$, the analysis fails to calculate a feasible γ value starting from $T_i = 40\,\mathrm{s}$ The worst-case drift and drift rate are $774\,\mathrm{m}$ and $24.7\,\mathrm{m/s}$, respectively. Thus, the performance degrades by a factor of 5.1 for the drift and 7.3 for the drift rate. This severe performance degradation shows the designs sensitivity with respect to simultaneous gain and phase perturbations. The complete analysis for a norm bound of 0.16 required $43\,\mathrm{min}$ on the same computer.

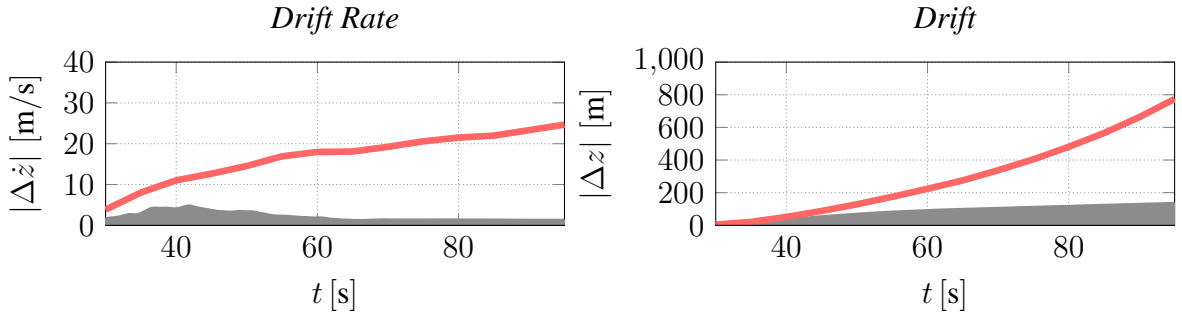

Figure 7: Results analysis with uncertainties: Monte Carlo Drift Minimal (——), LTV Drift Minimal (——)

A Monte Carlo simulation of the full nonlinear model extended with a disk margin type uncertainty validates the LTV IQC approach. Note that the dynamic uncertainty Δ represents an arbitrary stable and causal LTI system with $\|\Delta\|_\infty \leq b$. Hence, it requires a suitable parameterization for implementation. In this example, it is parameterized by 100 unique fourth-order LTI systems. The analysis is conducted over all parametrizations of Δ evaluated for each wind signal used in the nominal analysis. Fig. 7 shows the envelope of all Monte Carlo simulations up to $b = 0.16$, i.e. the maximum norm bound of the LTV IQC analysis. The maximum absolute drift off the trajectory is $136\,\mathrm{m}$, which corresponds to a performance degradation by a factor of 1.9. In case of the absolute drift rate, the identified maximum is $4.8\,\mathrm{m/s}$ $42\,\mathrm{s}$ into the ascent, i.e., a degradation by a factor of 3. The norm bound was further increased until the first departure occurred for $b = 0.21$ at $t = 32\,\mathrm{s}$ in to the flight. This b corresponds to a simultaneous gain phase perturbation of $\pm 3.7\,\mathrm{dB}$ and $\pm 23.7°$. However, oscillations in the pitch angle occurred from $b = 0.18$. Note that the Monte Carlo simulation appears less conservative due to the small wind disturbance and limited uncertainty set. However, the analysis still required approximately 2 and a half days parallelized on two standard desktop computer (identical to the previous analyses) for a single norm bound.
The LTV IQC analysis gives a good prediction of the (relative) performance degradation and provides an upper bound for the nonlinear analysis in a fraction of time. It also predicts the maximum tolerable

simultaneous gain and phase perturbation before a potential loss of the launch vehicle with good accuracy.

6 CONCLUSION

The paper demonstrates how modern LTV analysis methods can be used in the control design process of space launcher. Finite horizon LTV methods capture the behavior of the launcher along the trajectory accurately. Thus, they provide fast, reliable, and interpretable information about the effects of control design changes on the nominal and robust performance. As a complement to standard simulation-based methods, LTV methods can significantly accelerate the design process of which customers of ASTOS solutions will benefit.

REFERENCES

[1] M. Ganet-Schoeller, J. Desmariaux, and C. Combier, "Structured control for future european launchers," *AerospaceLab Journal*, vol. Issue 13, December 2017, ISSN: 2107–6596, 2017. DOI: 10.12762/2017.AL13-08.

[2] C. Roux and I. Cruciani, "Roll coupling effects on the stability margins for VEGA launcher," in *AIAA Atmospheric Flight Mechanics Conference and Exhibit*, American Institute of Aeronautics and Astronautics, Jun. 2007. DOI: 10.2514/6.2007-6630.

[3] P. Simplicio, S. Bennani, A. Marcos, C. Roux, and X. Lefort, "Structured singular-value analysis of the vega launcher in atmospheric flight," *Journal of Guidance, Control, and Dynamics*, vol. 39, no. 6, pp. 1342–1355, Jun. 2016. DOI: 10.2514/1.g000335.

[4] F. Biertümpfel and H. Pfifer, "Worst case gain computation of linear time-varying systems over a finite horizon," in *2nd Conference on Control Technology and Applications*, 2018.

[5] P. Seiler, R. M. Moore, C. Meissen, M. Arcak, and A. Packard, "Finite horizon robustness analysis of LTV systems using integral quadratic constraints," *Automatica*, vol. 100, pp. 135–143, Feb. 2019. DOI: 10.1016/j.automatica.2018.11.009.

[6] F. Biertümpfel, S. Bennani, and H. Pfifer, "Time-varying robustness analysis of launch vehicles under thrust perturbations," *Advanced Control for Applications*, vol. 3, no. 4, Nov. 2021. DOI: 10.1002/adc2.93.

[7] F. Biertümpfel, N. Pholdee, S. Bennani, and H. Pfifer, "Finite horizon worst case analysis of linear time-varying systems applied to launch vehicle," *IEEE Transactions on Control Systems Technology*, pp. 1–12, 2023. DOI: 10.1109/tcst.2023.3260728.

[8] J. Theis, H. Pfifer, and P. Seiler, "Robust modal damping control for active flutter suppression," *Journal of Guidance, Control, and Dynamics*, vol. 43, no. 6, pp. 1056–1068, Jun. 2020. DOI: 10.2514/1.g004846.

[9] F. Biertumpfel, J. Theis, and H. Pfifer, "Observer-based synthesis of finite horizon linear time-varying controllers," in *2022 American Control Conference (ACC)*, IEEE, Jun. 2022. DOI: 10.23919/acc53348.2022.9867184.

[10] J. Theis and H. Pfifer, "Observer-based synthesis of linear parameter-varying mixed sensitivity controllers," *International Journal of Robust and Nonlinear Control*, vol. 30, no. 13, pp. 5021–5039, Jul. 2020. DOI: 10.1002/rnc.5038.

[11] P. Seiler, "Stability analysis with dissipation inequalities and integral quadratic constraints," *IEEE Transactions on Automatic Control*, vol. 60, no. 6, pp. 1704–1709, Jun. 2015. DOI: 10.1109/tac.2014.2361004.

[12] M. Green and D. J. N. Limebeer, *Linear Robust Control*. Upper Saddle River, NJ, USA: Prentice-Hall, Inc., 1995, ISBN: 0-13-102278-4.

[13] F. Biertumpfel and H. Pfifer, "Worst case gain computation of linear time-varying systems over a finite horizon," in *2018 IEEE Conference on Control Technology and Applications (CCTA)*, IEEE, Aug. 2018. DOI: 10.1109/ccta.2018.8511591.

[14] H. Abou-Kandil, G. Freiling, V. Ionescu, and G. Jank, *Matrix Riccati Equations in Control and Systems Theory*. Birkhäuser Basel, 2003. DOI: 10.1007/978-3-0348-8081-7.

[15] MATLAB, *R2020b*. Natick, Massachusetts: The MathWorks Inc., 2020.

[16] H. Pfifer and P. Seiler, "Less conservative robustness analysis of linear parameter varying systems using integral quadratic constraints," *International Journal of Robust and Nonlinear Control*, vol. 26, no. 16, pp. 3580–3594, Feb. 2016. DOI: 10.1002/rnc.3521.

[17] J. Veenman, C. W. Scherer, and H. Köroğlu, "Robust stability and performance analysis based on integral quadratic constraints," *European Journal of Control*, vol. 31, pp. 1–32, Sep. 2016. DOI: 10.1016/j.ejcon.2016.04.004.

[18] A. L. Greensite, "Analysis and design of space vehicle flight control systems. volume i - short period dynamics," NASA Marshall Space Flight Center; Huntsville, AL, United States, Tech. Rep., 1967.

[19] ——, "Analysis and design of space vehicle flight control systems. volume i - short period dynamics," NASA Marshall Space Flight Center; Huntsville, AL, United States, Tech. Rep., 1967.

[20] "Manual of the icao standard artmosphere," International Civil Aviation Organization and Langley Aerodynamical Labratory, Tech. Rep., May 1954.

[21] NIMA, "Department of defense world geodetic system 1984, its definition and relationships with local geodetic systems," Department of Defense, Tech. Rep. 3, Jul. 1997.

[22] W. E. Wiesel, *Spaceflight dynamics*, English, 3rd ed. Beavercreek, Ohio : Aphelion Press, 2010, ISBN: 9781452879598 (pbk.)

[23] J. Orr, M. Johnson, J. Wetherbee, and J. McDuffie, "State space implementation of linear perturbation dynamics equations for flexible launch vehicles," in *AIAA Guidance, Navigation, and Control Conference*, American Institute of Aeronautics and Astronautics, Aug. 2009. DOI: 10.2514/6.2009-5962.

[24] F. M. Hoblit, *Gust Loads on Aircraft: Concepts and Applications*. American Institute of Aeronautics and Astronautics, Jan. 1988. DOI: 10.2514/4.861888.

[25] "Flying qualities of piloted airplanes u.s. military specification mil-f-8785c," U.S. Department of Defense, Tech. Rep., 1980.

[26] F. Biertümpfel and H. Pfifer, "Finite time horizon worst case analysis of launch vehicles," in *21st IFAC Symposium on Automatic Control in Aerospace*, 2019.

[27] A. L. Greensite, "Analysis and design of space vehicle flight control systems. volume vii - attitude control during launch," NASA Marshall Space Flight Center; Huntsville, AL, United States, Tech. Rep., 1967.

[28] P. Seiler, A. Packard, and P. Gahinet, "An introduction to disk margins [lecture notes]," *IEEE Control Systems*, vol. 40, no. 5, pp. 78–95, Oct. 2020. DOI: 10.1109/mcs.2020.3005277.